Valence Electronic Structures of CH_2BrCl and CF_2BrCl: Binding Energy Spectra and Electron Momentum Distributions

Zhong-Jun Li, Xu Shan, Xue-Feng Yang, Li-Qing Chen, Ke-Zun Xu, and Xiang-Jun Chen*

Hefei National Laboratory for Physical Sciences at Microscale and Department of Modern Physics, University of Science and Technology of China, Hefei, Anhui, 230026, People's Republic of China

Received: October 2, 2007; In Final Form: November 19, 2007

The binding energy spectra (BES) of valence shells of CH_2BrCl and CF_2BrCl have been measured at a series of different azimuthal angles by an (*e*, 2*e*) electron momentum spectrometer employing noncoplanar symmetric geometry at an impact energy of 1200 eV plus binding energy. The experimental momentum profiles (XMPs) are extracted from the sequential BES and compared with the theoretical ones calculated by using Hartree−Fock (HF) and density functional theory (DFT-B3LYP) calculations with 6-311G, 6-311++G**, and aug-cc-pVTZ basis sets. In general, the DFT-B3LYP calculations using the larger basis sets 6-311++G** and aug-cc-pVTZ describe the XMPs well for both molecules. Moreover, the pole strengths of main ionizations from the inner valence orbitals 2a′, 3a′, and 1a′ of CH_2BrCl are determined, and the controversial ordering of two outer valence orbitals 3a″ and 6a′ of CF_2BrCl has also been assigned unambiguously.

I. Introduction

CH_2BrCl and CF_2BrCl, two important halogenated molecules, are widely used in fire protection and refrigeration. They can be decomposed by solar ultraviolet radiation in the upper atmosphere to release atomic chlorine, bromine, and fluorine, which can react with stratosphere ozone layer and destroy it.[1−4] Therefore, the electronic structures of CH_2BrCl and CF_2BrCl have been the subject of many experimental and theoretical studies.[5−6,8−14]

The photoelectron spectra (PES) for the valence orbitals of CH_2BrCl had been studied by Novak et al.[5] using He I and He II radiation source. The assignments for the PES were presented by referring to the correlation with energy levels of either CH_2Cl_2 or CH_2Br_2 as well as the intensity variation of He I and He II PES. The first two bands at 10.77 and 11.06 eV in the PES were assigned to the ionizations from the bromine lone-pair orbitals, while the next one at 11.81 eV corresponded to the double-degenerate chlorine lone-pair orbitals. The other bands at 14.64, 15.39, 16.34, and 21.3 eV were assigned to the C−Br, C−Cl, and C−H bonding orbitals and C 2s orbital, respectively. Five years later, Novak and co-workers[6] extended the PES measurements over the inner valence region by using synchrotron radiation source. On the basis of their earlier studies mentioned above, the PES were assigned again by the molecular point group symmetry. In addition, the measured β spectra for 3a″ + 7a′ and 6a′ + 2a″ indicated that there were slight mixed characters of the different halogen lone pairs. Recently, He*-(2^3S) Penning ionization electron spectra (PIES) and He I ultraviolet PES as well as the outer valence Green function (OVGF) calculations[7] had been achieved by Tian et al.[8] Besides the assignments of six bands in the PIES, the first two bands were ascribed to the spin−orbit splitting components of bromine lone pairs on the basis of their experiments and OVGF calculations.

For CF_2BrCl, the PES of the outer valence orbitals had been measured by Doucet et al.[13] using He I radiation source and by Cvitaš et al.[14] using He I and He II radiation source. The simple assignments for the PES were presented by Doucet et al. according to the bonding characters of molecular orbitals. Subsequently, Cvitaš et al. reassigned the PES on the basis of the similarity to the PES of CF_2Cl_2 and CF_2Br_2. The bands at 11.51, 11.81, 12.89, 13.84, 15.94, 16.55, 19.07, 20.0, and 22.5 eV in the PES were assigned to the ionizations from 10a′, 6a″, 5a″ + 9a′, 8a′, 4a″ + 7a′, 6a′, 3a″ + 5a′, 2a″, and 4a′ orbitals, respectively. It is noted here that the ordering of 6a′ and 3a″ is in disagreement with our present theoretical calculations, and this will be discussed in this article.

To our best knowledge, no electron momentum spectroscopy (EMS) studies on CH_2BrCl and CF_2BrCl have ever been reported. EMS, also known as binary (*e*, 2*e*) spectroscopy, has been proven to be a powerful technique for exploring the electronic structures of atoms and molecules due to its unique ability to directly obtain not only the binding energy spectra but also the spherically averaged electron density distributions in momentum space for individual orbitals. EMS measurements, combined with the corresponding theoretical calculations, have offered a large amount of information and can be directly applied to evaluate the quality of wave functions obtained from quantum chemistry calculations,[15−21] analyze the bonding characters,[22] and assign the ordering of molecular orbitals[21,23−25] as well as explore the electron correlation effect in atoms and molecules.[21,23,26]

In this article, we report the first measurements on the binding energy spectra and the electron momentum distributions of CH_2BrCl and CF_2BrCl. The experimental momentum distributions are compared with the theoretical ones calculated by using different methods with different basis sets. The controversial ordering of 6a′ and 3a″ of CF_2BrCl is determined, and the ionization pole strengths for the inner valence orbitals of CH_2BrCl are estimated. Furthermore, the fluorine-substituted effects on the energy levels and the electron density distributions are discussed by comparing the results of CH_2BrCl and CF_2BrCl.

* Corresponding author. E-mail: xjun@ustc.edu.cn.

10.1021/jp709645d CCC: $40.75
Published on Web 01/12/2008

II. Experimental and Theoretical Background

EMS is based on a kinematically complete (e, $2e$) collision experiment in which an electron from target atoms or molecules is cleanly knocked out by a high-energy incident electron and the residual ion acts as a spectator. Conservation of energy and momentum requires that

$$\epsilon = E_0 - E_1 - E_2 \quad (1)$$

$$\mathbf{p} = \mathbf{p}_1 - \mathbf{p}_2 - \mathbf{p}_0 \quad (2)$$

where ϵ and $\mathbf{p}$ are the binding energy and the momentum of the target electron, and E_i and $\mathbf{p}_i$ ($i = 0, 1, 2$) are the energies and the momenta of the incident and two outgoing electrons, respectively. Thus, by detecting the two outgoing electrons in coincidence, the binding energy and the momentum of the target electron can be determined.

The details of the present EMS spectrometer employing symmetric noncoplanar geometry have been described elsewhere,[27] and hence only a brief description will be given here. The gas-phase target molecules are ionized by an impact with a high-energy electron beam ($E_0 = 1200$ eV + binding energy). The scattered and ionized electrons having essentially equal energy, and the same polar angles ($\theta_1 = \theta_2 = \theta = 45°$) are received by two hemispherical electron energy analyzers with a five-element cylindrical retarding lens and are detected in coincidence by one-dimensional position-sensitive detectors. The relative azimuthal angle ϕ between the two outgoing electrons is variable over a wide range ($0° \sim \pm 30°$) by rotating one energy analyzer around the direction of the incident electron beam and keeping the other fixed. In this kinematic arrangement, the quantity p of target electron momentum is related to the relative azimuthal angle ϕ by

$$p = \{(2p_1 \cos\theta - p_0)^2 + [2p_1 \sin\theta \sin(\phi/2)]^2\}^{1/2} \quad (3)$$

In EMS experiment, the completely observable quantity is the triple differential cross section (TDCS). With the plane wave impulse approximation (PWIA), the TDCS (σ_{EMS}) for randomly oriented gas-phase molecules is formulated by[15−18,28]

$$\sigma_{EMS} \propto \int d\Omega\, |\langle \mathbf{p}\Psi_f^{N-1} | \Psi_i^N \rangle|^2 \quad (4)$$

where Ψ_f^{N-1} and Ψ_i^N are the total electronic wave functions for the final ion state and the target molecule ground (initial) state, and $\mathbf{p}$ is the momentum of target electron prior to knockout. The overlap of the ion and neutral wave functions in eq 4 is known as the Dyson integral.

Further, by using the target Hartree−Fock approximation (THFA)[28−33] or the target Kohn−Sham approximation (TKSA)[34−36] in which the Dyson integral is approximated to be a neutral state canonical HF or KS orbital, the TDCS can be simplified by

$$\sigma_{EMS} \propto S_q^f \int d\Omega\, |\varphi_q(\mathbf{p})|^2 \quad (5)$$

where S_q^f is called spectroscopic factor or pole strength which is the possibility of finding a one-hole configuration in the final state f, and $\varphi_q(\mathbf{p})$ is the one-electron canonical HF or KS wave function in momentum space for the qth orbital from which the electron is ionized. The integral in eq 5 is known as the spherically averaged electron momentum distributions.

In the present work, the theoretical spherically averaged momentum distributions, i.e., the theoretical momentum profiles (TMPs), for the valence orbitals of CH_2BrCl and CF_2BrCl are obtained according to eq 5 within the target HF or KS approximation. The corresponding position-space canonical HF or KS orbital wave functions are calculated using HF and DFT-B3LYP methods with 6-311G, 6-311++G**, and aug-cc-pVTZ basis sets under the Gaussian 98 program.[37] The keyword B3LYP refers to Becke's three-parameter hybrid functional combined with Lee−Yang−Parr correlation functional.[38,39] It should be noted that the HF calculation only contains the exchange effect resulting from the electronic fermion nature, while in the DFT-B3LYP calculation, not only the exchange effect but also the correlation interaction is included. In addition, the second-order Møllet−Plesset perturbation (MP2) method with aug-cc-pVTZ basis sets is employed to optimize the molecular geometric parameters, and the OVGF method[7] with aug-cc-pVTZ is performed to obtain the ionization potentials and pole strengths of valence orbitals for both molecules.

Before the normal experiments, the energy and momentum resolution of the present EMS spectrometer was determined to be ~1.1 eV [full width at half-maximum (fwhm)] and ~0.15 au, respectively, by measuring Ar 3p ionization. The CH_2BrCl and CF_2BrCl samples, with about 99.6% stated purity, were degassed by several freeze−pump−thaw cycles,[40] and no impurities were observed in any of the binding energy spectra.

III. Results and Discussion

A. Binding Energy Spectra. CH_2BrCl and CF_2BrCl both belong to the C_s point group symmetry, and their ground state electronic configurations are as follows:

$$CH_2BrCl:\ (core)^{40}\underbrace{(1a')^2(2a')^2(3a')^2}_{\text{inner valence}}\underbrace{(1a'')^2(4a')^2(5a')^2(2a'')^2(6a')^2(7a')^2(3a'')^2}_{\text{outer valence}}$$

$$CF_2BrCl:\ (core)^{44}\underbrace{(1a')^2(1a'')^2(2a')^2(3a')^2(4a')^2}_{\text{inner valence}}$$

$$\underbrace{(2a'')^2(5a')^2(6a')^2(3a'')^2(4a'')^2(7a')^2(8a')^2(9a')^2(5a'')^2(6a'')^2(10a')^2}_{\text{outer valence}}.$$

The orderings of the valence orbitals for CH_2BrCl and CF_2BrCl listed above are adopted from the HF calculations using aug-cc-pVTZ basis sets.

The binding energy spectra (BES) of CH_2BrCl and CF_2BrCl have been measured at 16 different azimuthal angles ϕ. Figure 1 and Figure 2 show their individual BES at (a) $\phi = 0°$, (b) $\phi = 8°$, and (c) the summed spectra for all angles. It can be seen from the figures that the data for CH_2BrCl has larger statistical error bars than the data for CF_2BrCl although the accumulation time is about the same order. The reason lies in two aspects: much lower vapor pressure and lower cross section for CH_2BrCl than those for CF_2BrCl. Because of the poor energy resolution of our spectrometer, only five resolved bands for both molecules have been observed in the BES. Gaussian peaks are used to fit these resolved bands, the positions of Gaussian peaks are referred to the ionization potentials from the PES studies,[6,14] and the widths of them are the convolutions of the present instrumental energy resolution and Franck−Condon width of the corresponding ionization bands estimated by the PES.[5,6,14] Small adjustments have been applied to compensate for the asymmetry of the Franck−Condon profiles. The deviations of the peak positions from the PES values of the ionization potentials due to this asymmetry are determined by convoluting the Franck−Condon profiles with the present instrumental function. For example, the determined deviation for the ionization band at about 16.8 eV for CF_2BrCl is 0.2 eV, as shown in Table 2.

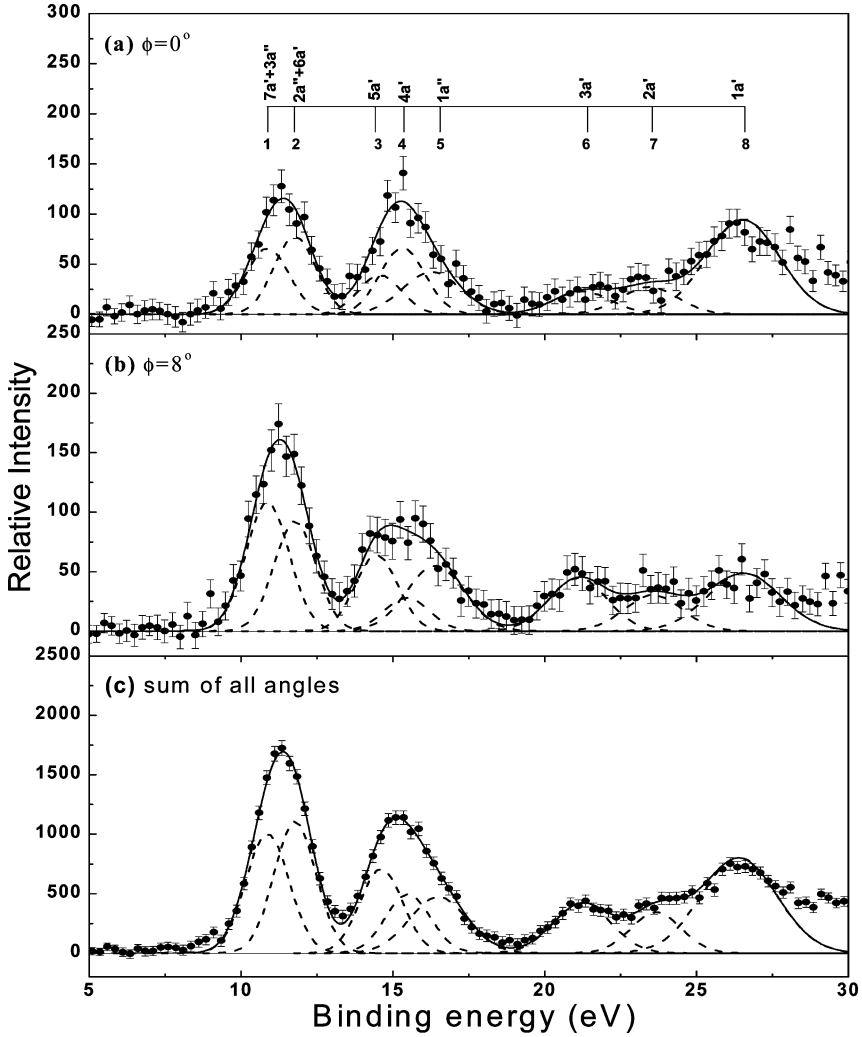

Figure 1. Binding energy spectra of CH_2BrCl at (a) $\phi = 0°$, (b) $\phi = 8°$, and (c) the sum of all 16 different ϕ angles. The dotted lines indicate the Gaussian peaks, and the solid line is the summed fit. Vertical bars 1−8 correspond to the ionizations from 7a′ + 3a″, 2a″ + 6a′, 5a′, 4a′, 1a″,3a′, 2a′, and 1a′ valence orbitals.

For CH_2BrCl the five resolved bands correspond to the ionizations from seven outer valence and three inner valence orbitals. As shown in Figure 1, the first band is fitted to two Gaussian peaks which are contributed from the bromine and chlorine lone-pair orbitals and assigned to 7a′ + 3a″ and 6a′ + 2a″ orbitals, respectively. The second one is fitted to three Gaussian peaks which are assigned to the C−Br (5a′), C−Cl (4a′), and C−H (1a″) bonding orbitals, respectively. The last three are fitted to three individual Gaussian peaks which correspond to the three inner valence orbitals 3a′, 2a′, and 1a′. The positions of above eight Gaussian peaks are at 10.87, 11.78, 14.62, 15.50, 16.50, 21.23, 23.67, and 26.40 eV.[6]

Like CH_2BrCl, five resolved bands are observed in the BES of CF_2BrCl, and these are also fitted to eight Gaussian peaks, as presented in Figure 2. However, the components of each band are different from CH_2BrCl due to the fluorine substitution. The first band is contributed from the bromine lone-pair orbitals (10a′ and 6a″) and is fitted to one Gaussian peak. The second one is fitted to two Gaussian peaks which are corresponding to the ionization from the chlorine lone pairs (5a″ + 9a′) and the C−Br bonding orbitals (8a′). The third one is ascribed to the transitions from the three fluorine lone-pair orbitals and is fitted to two Gaussian peaks (4a″ + 7a′ and 3a″). The fourth one is fitted to two Gaussian peaks which are contributed from the fluorine lone-pair, C−Cl and C−F bonding orbitals (6a′ + 5a′ and 2a″), respectively. The last one corresponds to the ionization from the inner valence orbital of 4a′ and is fitted to an individual Gaussian peak. The positions of Gaussian peaks are at 11.65, 12.9, 13.9, 16.0, 16.8, 19.0, 20.2, and 22.65 eV.[14]

Tables 1 and 2 summarize the present and the previous theoretical and experimental ionization potentials of the valence orbitals for CH_2BrCl and CF_2BrCl.[5−6,8,13,14] It can be seen from the tables that our calculated ionization potentials using OVGF/aug-cc-pVTZ for both molecules are consistent with those of the previous experimental results. But for some molecular orbitals, the different studies offer the discrepant orbital orderings. For CH_2BrCl the first two bands in the PES were assigned to 7a′ and 3a″ orbitals by Novak et al.,[5,6] while the recent PIES study of Tian et al.[8] given the reverse results (3a″ and 7a′). For CF_2BrCl the discrepancy of orbital orderings lied in 3a″ and 6a′. Doucet et al.[13] and Cvitaš et al.[14] both gave the ordering of 6a′ and 3a″ in the order of increasing ionization energy, which disagrees with our present OVGF calculations. The reassignment of 6a′ and 3a″ ordering has been made by comparing their TMPs with the experiment in section B. However, for 7a′ and 3a″ of CH_2BrCl, due to their very close energy space, the reassignment is beyond our present EMS spectrometer.

In order to explore the fluorine-substituted effect on orbital ionization potentials, the correlation diagram for the occupied valence orbitals of CH_2BrCl and CF_2BrCl is given in Figure 3, in which the ionization potentials are referred to the measured results of Novak et al.[5] and Cvitaš et al.,[14] respectively. It is

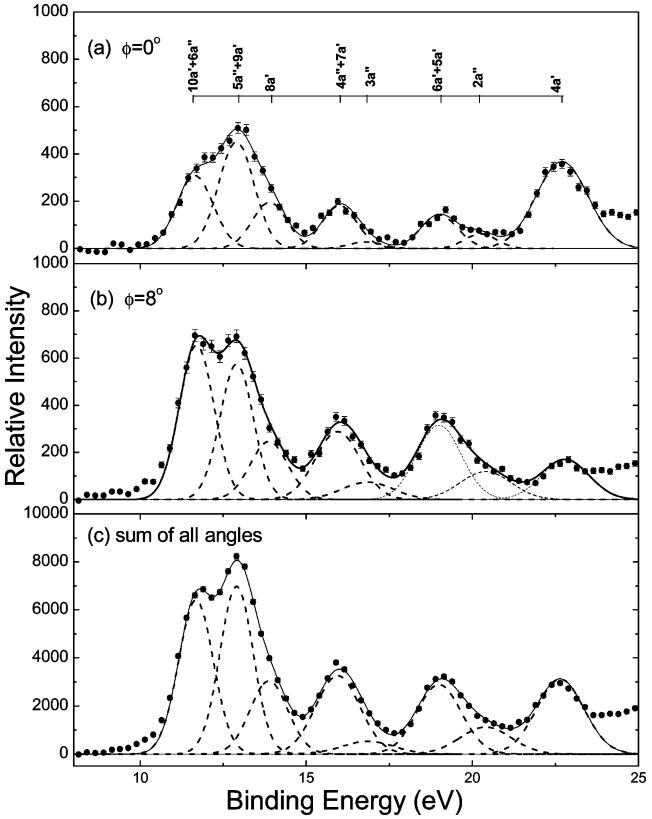

Figure 2. Binding energy spectra of CF_2BrCl at (a) $\phi = 0°$, (b) $\phi = 8°$, and (c) the sum of all 16 different ϕ angles. The dotted lines indicate the Gaussian peaks, and the solid line is the summed fit. Vertical bars 1−8 correspond to the ionizations from 10a′ + 6a″, 5a″ + 9a′, 8a′, 4a″ + 7a′, 3a″, 6a′ + 5a′, 2a″, and 4a′ valence orbitals.

clear that the orbital ionization potentials of CF_2BrCl become higher than those of the correlated orbitals of CH_2BrCl except for 8a′ orbital. The lower ionization potential of 8a′ orbital may be ascribed to the out-of-phase combination of the C−Br group and the fluorine lone pairs. Moreover, two split bands with an interval of about 0.3 eV have been observed in PES[6,14] for the bromine lone-pair ionizations of both molecules. For CH_2BrCl, Tian et al.[8] assigned the split to the spin−orbit coupling effect of bromine according to the band shape of PES and PIES, the slope of the collision energy dependence of partial ionization cross sections, and the split energy from the OVGF calculation. But for CF_2BrCl, as observed in PES,[13] the first split band is weaker in intensity than the second one, which suggests that a strong intramolcular interaction is expected to occur in this molecule. Our OVGF calculations predict the split energy of bromine lone pairs in CF_2BrCl is 0.23 eV, larger than that in CH_2BrCl (0.03 eV).[8] Because the OVGF calculations do not consider the spin−orbit coupling effect, our calculated results indicate that the intramolcular interactions in CF_2BrCl become more remarkable than in CH_2BrCl. This may be attributed to the fluorine-substituted effect.[41]

B. Electron Momentum Distributions. As mentioned above, five resolved bands in BES for CH_2BrCl and CF_2BrCl are fitted by eight Gaussian peaks, and hence only the experimental momentum profiles (XMPs) for these Gaussian peaks have been obtained by deconvoluting the same Gaussian peak from the sequentially measured BES at different azimuthal angles ϕ and plotting area under the corresponding fitted peak as a function of momentum p (i.e., ϕ angles). In order to compare the XMP with the TMPs, the instrumental momentum resolution of 0.15 au has been convoluted into the TMPs utilizing the Gaussian-weighted planar grid method (GWPG).[42] On the other hand, the XMP and the TMPs are placed on a common intensity scale by normalizing the XMPs of the outermost orbital to the corresponding TMPs since its ionization pole strength is close to unity. In this work, the normalization factors for both molecules are obtained by comparing the XMP of the first band with their TMPs obtained using B3LYP method with aug-cc-pVTZ basis set.

Figures 4 and 5 present the XMPs of the valence orbitals for CH_2BrCl and CF_2BrCl, together with the corresponding TMPs calculated using HF and B3LYP methods with 6-311G, 6-311++G** and aug-cc-pVTZ basis sets. In addition, the electron density images for the individual orbitals in position space calculated using B3LYP method with aug-cc-pVTZ basis set are also shown in top right corner of each graph. The detailed discussion about the electron momentum profiles for both molecules will be introduced according to the category of the molecular orbital character.

1. Bromine and Chlorine Lone-Pair MOs for CH_2BrCl and CF_2BrCl. As shown in Figure 4a, the summed XMP of the first two orbitals 7a′ and 3a″ for CH_2BrCl displays a p-type character having a maximum at p ∼ 0.52 au. The TMPs calculated by HF and B3LYP methods with aug-cc-pVTZ and 6-311++G** basis sets are in good agreement with the XMP. But the TMPs obtained using the small basis set 6-311G cannot predict the XMP well both in shape and magnitude. Moreover, the XMP of 7a′ + 3a″ is obviously more diffuse than that of atomic bromine 4p (denoted by shot dash-dotted curve in Figure 4a). This indicates that 7a′ and 3a″ may not be pure bromine lone-pair character. Our calculated orbital electron density images also show these two orbitals are contributed from not only the bromine lone-pair systems but also some chlorine ones, which agree with the prediction of Novak et al.[5,6]

Similar to the case of CH_2BrCl, the summed XMP of the first two orbitals 10a′ and 6a″ for CF_2BrCl in Figure 5a exhibits a p-type character with a maximum at $p \sim 0.61$ au, and all the TMPs describe the XMP well except for underestimating the magnitude of the XMP at the origin of momenta. Compared with the component of atomic bromine 4p (having a maximum at $p \sim 0.53$ au), the XMP of 10a′ + 6a″ is more diffuse, and its maximum position obviously moves toward the larger momentum ($p \sim 0.61$ au). This is understandable because these two orbitals are also the contribution of the bromine lone pairs with some mixture of chlorine as the orbital electron density images exhibit.

For the second two orbitals of 2a″ and 6a′ of CH_2BrCl and 5a″ and 9a′ of CF_2BrCl, the XMPs both exhibit p-type characters, as shown in Figures 4b and 5b. The former has a maximum at $p \sim 0.65$ au and the latter at $p \sim 0.46$ au. They are both obviously different from those of atomic chlorine 3p with a maximum at $p \sim 0.59$ au, which should be ascribed to the contribution of chlorine and bromine lone-pair systems in these molecular orbitals. On the other hand, the TMPs of 2a″ + 6a′ for CH_2BrCl calculated using B3LYP method with the large basis sets aug-cc-pVTZ and 6-311++G** is consistent with the experiments, but other TMPs underestimate the magnitude of the XMP in the region $p < 0.8$ au. For CF_2BrCl, all the TMPs of 5a″ + 9a′, especially the TMPs calculated using the B3LYP method with aug-cc-pVTZ and 6-311++G** basis sets, give a good description of the XMP.

As mentioned above, the first four orbitals of CH_2BrCl and CF_2BrCl have similar orbital components, i.e., the mixture of bromine and chlorine lone pairs, and their XMPs all exhibit p-type distributions. But due to the fluorine-substituted effect, there are some distinct differences observed in the XMPs of

TABLE 1: Ionization Potentials for the Valence Orbitals of CH_2BrCl are Listed in Parentheses (in eV) and Pole Strengths in Square Brackets

experiments				theoretical calculations	
HeIIPES[5]	SRPES[6]	PIES[8]	present EMS	OVGF/6-311+G(d,p)[8]	present OVGF/aug-cc-pVTZ
7a′ (10.77)	7a′(10.77)	3a″(10.75)	3a″(10.87)	3a″(10.62) [0.94]	3a″(10.73) [0.92]
3a″ (11.06)	3a″ (11.06)	7a′ (11.08)	7a′ (10.87)	7a′ (10.65) [0.94]	7a′ (10.73) [0.92]
6a′ (11.81)	6a′ (11.81)	6a′ (11.79)	6a′ (11.78)	6a′ (11.43) [0.92]	2a″ (11.49) [0.92]
2a″ (11.81)	2a″ (11.81)	2a″ (11.79)	2a″ (11.78)	2a″ (11.50) [0.92]	6a′ (11.59) [0.92]
5a′ (14.54)	5a′ (14.54)	5a′ (14.63)	5a′ (14.62)	5a′ (14.40) [0.92]	5a′ (14.31) [0.91]
4a′ (15.39)	4a′ (15.39)	4a′ (15.40)	4a′ (15.50)	4a′ (15.28) [0.91]	4a′ (15.14) [0.91]
1a″ (16.34)	1a″ (16.34)	1a″ (16.32)	1a″ (16.50)	1a″ (16.59) [0.90]	1a″ (16.6) [0.91]
3a′ (21.30)	3a′ (21.30)		3a′ (21.23) [0.74]		3a′ (21.63) [0.83]
	2a′ (23.50)		2a′ (23.67) [0.39]		
	1a′ (26.60)		1a′ (26.40) [0.30]		

TABLE 2: Ionization Potentials for the Valence Orbitals of CF_2BrCl are Listed in Parentheses (in eV) and Pole Strengths in Square Brackets

experiments			present calculations	
He I PES[13]	He II PES[14]	present EMS	HF/aug-cc-pVTZ	OVGF/aug-cc-pVTZ
10a′ (11.83)	10a′ (11.51)	10a′ (11.65)	10a′ (12.36)	10a′ (11.45) [0.92]
6a″ (11.83)	6a″ (11.81)	6a″ (11.65)	6a″ (12.59)	6a″ (11.68) [0.92]
5a″ (12.90)	5a″ (12.89)	5a″ (12.9)	5a″ (13.76)	5a″ (12.49) [0.91]
9a′ (12.90)	9a′ (12.89)	9a′ (12.9)	9a′ (13.78)	9a′ (12.61) [0.91]
8a′ (13.83)	8a′ (13.84)	8a′ (13.9)	8a′ (14.94)	8a′ (13.66) [0.92]
7a′ (16.0)	7a′ (15.94)	7a′ (16.0)	7a′ (17.46)	7a′ (15.77) [0.91]
4a″ (16.0)	4a″ (15.94)	4a″ (16.0)	4a″ (18.51)	4a″ (16.12) [0.92]
6a′ (16.60)	6a′ (16.55)	3a″ (16.8)	3a″ (19.42)	3a″ (16.81) [0.92]
3a″ (18.8)	3a″ (19.00)	6a′ (19.0)	6a′ (21.14)	6a′ (18.68) [0.91]
5a′ (18.8)	5a′ (19.00)	5a′ (19.0)	5a′ (21.26)	5a′ (18.81) [0.91]
2a″ (19.8)	2a″ (20.00)	2a″ (20.2)	2a″ (21.92)	2a″ (19.81) [0.91]
	4a′ (22.50)	4a′ (22.65)	4a′ (25.26)	4a′ (22.74) [0.86]

the corresponding orbitals. For the first two orbitals, the maximum of the XMP for CF_2BrCl locates at larger momentum ($p \sim 0.61$ au) than that for CH_2BrCl ($p \sim 0.52$ au). While for the next two orbitals, the maximum of the XMP for CF_2BrCl positions at smaller momentum ($p \sim 0.46$ au) than that for CH_2BrCl ($p \sim 0.65$ au).

2. Fluorine Lone-Pair Orbitals for CF_2BrCl. The calculated electron density images presented in Figure 5d−f suggest that the orbitals 7a′, 4a″, 3a″, and 6a′ of CF_2BrCl are mainly ascribed to the fluorine lone-pair orbitals, which do not exist in CH_2BrCl. As shown in Figure 5d, the summed XMP of 4a″ and 7a′ orbitals displays two maxima at $p \sim 0.55$ au and $p \sim 1.3$ au and a minimum at $p \sim 1.0$ au. All the calculated TMPs predict the shape of the XMPs well but largely underestimate the magnitude in the low momentum region, and a similar underestimation has been observed in the fluorine lone-pair orbitals of other fluomethanes.[23,43]

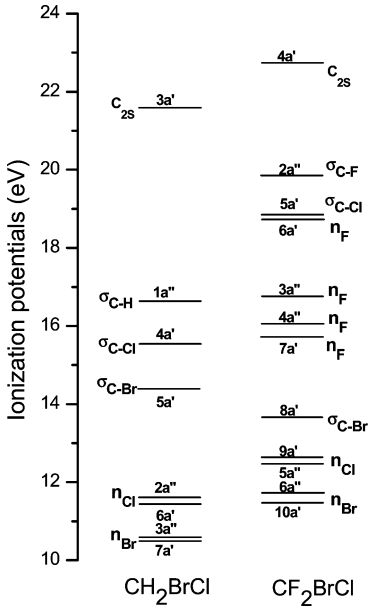

Figure 3. Correlation diagram for the occupied valence orbitals of CH_2BrCl and CF_2BrCl.

The XMP for the fifth band at 16.8 eV in BES is shown in Figure 5e. The PES works of Doucet et al.[13] Cvitaš et al.[14] both assigned this band to 6a′, but our theoretical calculations assign it to 3a″. Therefore, the TMPs of 3a″ and 6a′ are both presented and compared with the XMP in Figure 5e. It is clear in the figure that the TMPs of 3a″ is of good agreement with the experiment, and hence this band should be assigned to 3a″. For 6a′ orbital, the last fluorine lone pairs, due to the close energy space with other orbitals, the summed XMP of 6a′ + 5a′ + 2a″ will be discussed in the next section.

3. Bonding Orbitals for CH_2BrCl and CF_2BrCl. Besides the halogen lone-pair orbitals, the remainder outer valence orbitals for CH_2BrCl and CF_2BrCl are the bonding orbitals. As shown in Figures 4c and 5c, the electron density images show 5a′ of CH_2BrCl and 8a′ of CF_2BrCl are both mainly σ_{C-Br} bonding orbitals with a small chlorine components while 8a′ also includes a small fluorine lone pairs. The XMP of 5a′ of CH_2BrCl has a maximum at $p \sim 0.75$ au, and the TMP calculated by B3LYP method with aug-cc-pVTZ and 6-311++G** basis sets gives a good description of the XMP while the other TMPs underestimate the intensity of the XMP in the low momentum region. The XMP of 8a′ of CF_2BrCl displays a p-type character with two maxima at $p \sim 0.4$ au and $p \sim 1.2$ au, obviously different from that of 5a′ of CH_2BrCl. The occurrence of the second maximum should be ascribed to the contribution of the fluorine lone pairs to 8a′ orbital of CF_2BrCl. In addition, all the TMPs of 8a′ largely underestimate the magnitude of XMP in the low momentum region.

The orbital electron density images in Figure 4d,e show the nature of 4a′ and 1a″ of CH_2BrCl are σ_{C-Cl} and σ_{C-H} bonding

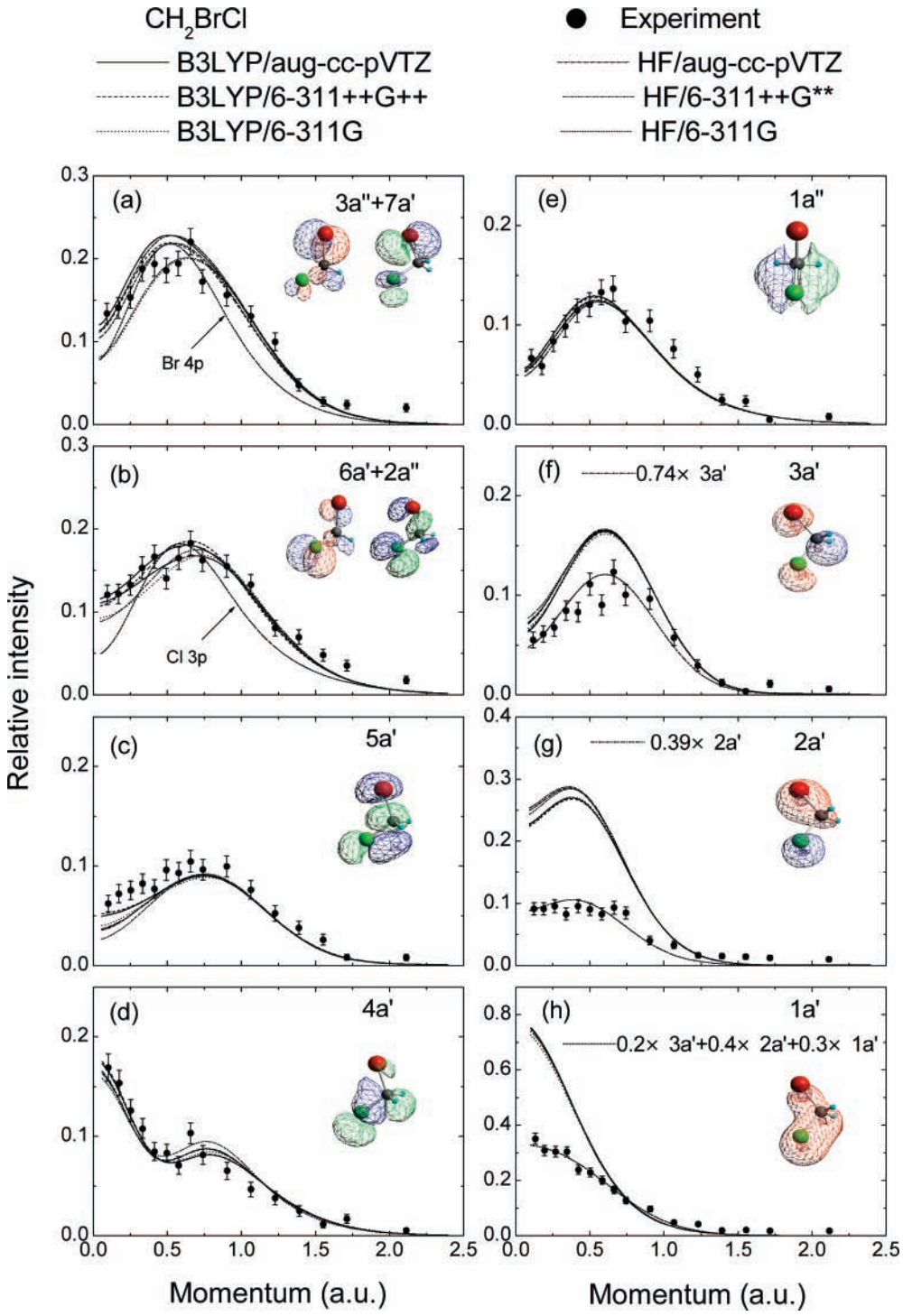

Figure 4. Measured and calculated spherically averaged momentum profiles for (a) 3a″ + 7a′, (b) 6a′ + 2a″, (c) 5a′, (d) 4a′, (e) 1a″, (f) 3a′, (g) 2a′, and (h) 1a′ orbitals of CH_2BrCl. The individual orbital electron density images in position space calculated using B3LYP/aug-cc-pVTZ are shown in the top right corner of each graphs, and the TMPs of atomic Br 4p and Cl 3p calculated using B3LYP/aug-cc-pVTZ are presented in (a) and (b). The TMPs calculated using B3LYP/aug-cc-pVTZ multiplied by the pole strengths are represented in (f), (g), and (h) by the shot dash-dotted curves.

orbitals, respectively. The XMP of 4a′ displays an sp-type character with a minimum at $p \sim 0.5$ au and a second maximum at $p \sim 0.8$ au. The XMP of 1a″ exhibits a p-type character having a maximum at $p \sim 0.55$ au. For this two orbitals, all the TMPs well reproduce the shape and magnitude of the XMP, especially the TMPs obtained using B3LYP method with aug-cc-pVTZ and 6-311++G** basis sets.

For CF_2BrCl, 5a′ and 2a″ are essentially σ_{C-Cl} and σ_{C-F} bonding orbitals, respectively. Because of the low resolution of the present spectrometer, they are not resolved from the fluorine lone-pair orbital 6a′. Hence, the summed XMP of 6a′ + 5a′ + 2a″ is presented in Figure 5f. It exhibits a p-type character with a maximum at $p \sim 0.85$ au, and all the TMPs give a similar shape but underestimate the magnitude at the region $p < 0.55$ au.

4. Inner Valence MOs for CH_2BrCl and CF_2BrCl. As shown in Figure 4f−h, the inner valence orbitals 3a′, 2a′, and 1a′ of CH_2BrCl are mainly from the C 2s, Br 4s, and Cl 3s contributions. The XMPs of 3a′ and 2a′ are both p-type in nature, while the XMP of 1a′ is of s-type. For these orbitals, the

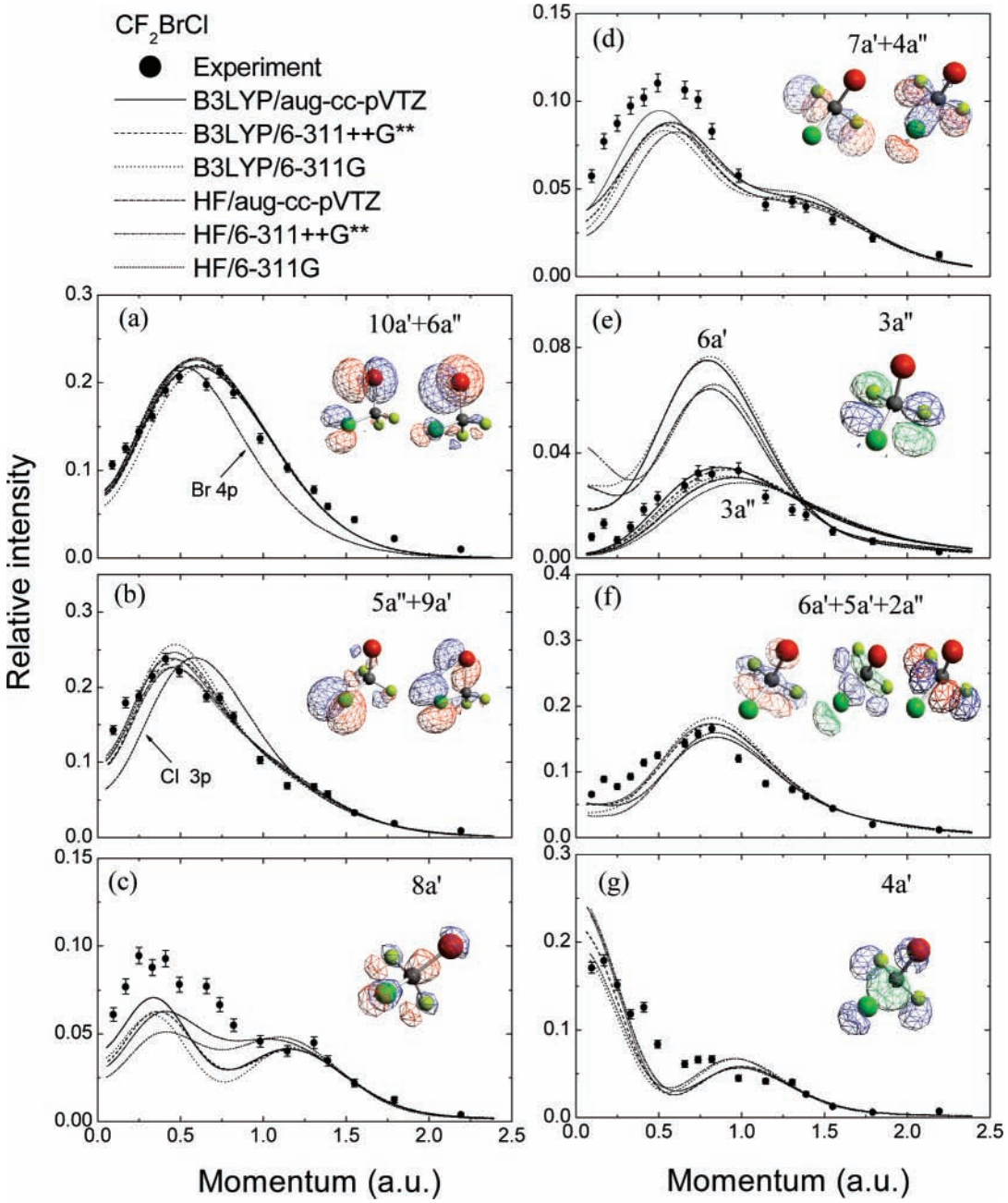

Figure 5. Measured and calculated spherically averaged momentum profiles for (a) 10a′ + 6a″, (b) 5a″ + 9a′, (c) 8a′, (d) 4a″ + 7a′, (e) 3a″, (f) 6a′ + 5a′ + 2a″, and (g) 4a′ orbitals of CF_2BrCl. The individual orbital electron density images in position space calculated using B3LYP/aug-cc-pVTZ are shown in the top right corner of each graphs. The TMPs of atomic Br 4p and Cl 3p calculated using B3LYP/6 aug-cc-pVTZ are also presented in (a) and (b).

intensities of the TMPs are much higher than the experimental ones. When the TMPs are multiplied by a factor, they are in good agreement with the XMP, as shown by the shot dash-dotted curves in the figures. The factor is approximately equivalent to the pole strength of the transition. For the transitions from 3a′ and 2a′ orbitals, the factors are 0.74 and 0.39, respectively. Such small pole strengths indicate there are significant many-body effects in the ionization processes, and the one-electron orbital ionization picture well describing the ionizations of outer valence orbitals is not adequate to describe the ionizations of inner valence orbitals. But for the 1a′ orbital, no matter how to change the value of the scaling factor, the TMPs of 1a′ orbital still disagrees with the XMP. In view of the strong many-body effects of the 3a′ and 2a′ ionizations, the summed TMPs contributed from 1a′, 2a′, and 3a′ orbitals is in accordance with the experiments. These suggest that the correlative satellite lines of the 3a′ and 2a′ ionizations maybe contribute to the main peak of 1a′ ionization. Although we list the calculated pole strength, 0.83 (OVGF/aug-cc-pVTZ) in Table 1 for 3a′ ionization, the result is unreliable for such a pole strength calculated with OVGF method which is less than 0.85. The quantitative calculations of the pole strengths are thus expected for these transitions.

For CF_2BrCl, the last band at 22.65 eV in BES is from the ionization of the inner valence orbital 4a′, and its XMP in Figure 5g shows an sp-type character. This is understandable because 4a′ orbital is mainly contributed from the C 2s orbital and a small fluorine lone pair as shown in its electron density images. All the theoretical calculations predict the shape of the XMP well, and some differences appear near $p \sim 0.5$ au.

IV. Summary

In this article, we have reported the first EMS measurements on the binding energy spectra and the electron momentum distributions of the valence orbitals for CH_2BrCl and CF_2BrCl. The experimental momentum profiles are compared with the theoretical ones calculated by using HF and B3LYP methods with 6-311G, 6-311++G**, and aug-cc-pVTZ basis sets. Generally, the calculations using B3LYP method with larger basis sets aug-cc-pVTZ and 6-311++G** are in good agreement with the experiments. Furthermore, the pole strengths of ionizations from the inner valence orbitals 3a′, 2a′, and 1a′ of CH_2BrCl have been obtained, and the small pole strengths indicate that significant many-body effects occur in the ionizations of inner valence orbitals. The controversial ordering between 3a″ and 6a′ of CF_2BrCl has also been determined by comparing their TMPs with the XMP; i.e., the fifth peak at 16.8 eV in BES should be assigned to 3a″, rather than 6a′. In addition, the fluorine-substituted effects on the energy levels and the electron density distributions have been analyzed by comparing the results of CH_2BrCl and CF_2BrCl.

Acknowledgment. This work was supported by National Natural Science Foundation of China (Grant No.10474090 and 10734040), and Xiang-Jun Chen thanks Ministry of Education of China for the Program for New Century Excellent Talents in University. The authors also gratefully acknowledge Professor C. E. Brion from the University of British Columbia (UBC) in Canada for supplying the HEMS and RESFOLD programs.

References and Notes

(1) Yung, Y. L.; Pinto, J. P.; Watson, R. J.; Sander, S. P. *J. Atmos. Sci.* **1980**, *37*, 339.
(2) Rowland, F. S. *Annu. Rev. Phys. Chem.* **1991**, *42*, 731.
(3) Bilde, M.; Wallington, T. J.; Ferronato, C.; Orlando, J. J.; Tyndall, G. S.; Estupinan, E.; Haberkorn, S. *J. Phys. Chem. A* **1998**, *102*, 1976.
(4) Bilde, M.; Sehested, J.; Nielsen, O. J.; Wallington, T. J.; Meagher, R. J.; McIntosh, M. E.; Piety, C. A.; Nicovich, J. M.; Wine, P. H. *J. Phys. Chem. A* **1997**, *101*, 8035.
(5) Novak, I.; Cvitaš, T.; Klasinc, L. *J. Chem. Soc., Faraday Trans. 2* **1981**, *77*, 2049.
(6) Novak, I.; Benson, J. M. *Chem. Phys.* **1986**, *107*, 129.
(7) (a) Cederbaum, L. S. *J. Phys. B* **1975**, *8*, 290. (b) von Niessen, W.; Schirmer, J.; Cederbaum, L. S. Comput. *Phys. Rep.* **1984**, *1*, 57. (c) Zakrzewski, V. G.; Ortiz, J. V.; Nichols, J. A.; Heryadi, D.; Yeager, D. L.; Golab, J. T. *Int. J. Quantum Chem.* **1996**, *60*, 29.
(8) Tian, S. X.; Kishimoto, N.; Ohno, K. *J. Phys. Chem. A* **2003**, *107*, 2137.
(9) Baum, G.; Huber, J. R. *Chem. Phys. Lett.* **1993**, *213*, 427.
(10) Huang, J. H.; Xu, D. D.; Francisco, J. S.; Jackson. W. M. *J. Chem. Phys.* **2003**, *119*, 3661.
(11) Konaka, S.; Kiyoto, K.; Yamamoto, K.; Suzuki, N.; Kimura, M. *J. Mol. Struct.* **1984**, *125*, 143.
(12) Rozgonyi, T.; Gonzlez, L. *J. Phys. Chem. A* **2006**, *110*, 10251.
(13) Doucet, J.; Gilbert, R.; Sauvageau, P.; Sandorfy, C. *J. Chem. Phys.* **1975**, *62*, 366.
(14) Cvitaš, T.; Klasinc, L.; Novak, I. *Int. J. Quantum Chem. Quantum Chem. Symp.* **1980**, *14*, 305.
(15) McCarthy, I. E.; Weigold, E. *Rep. Prog. Phys.* **1991**, *54*, 789.
(16) Brion, C. E. *Int. J. Quantum Chem.* **1986**, *29*, 1397.
(17) Coplan, M. A.; Moore, J. H.; Doering, J. P. *Rev. Mod. Phys.* **1994**, *66*, 985.
(18) Leung, K. T. In *Theoretical Models of Chemical Bonding, Part 3*; Maksic, Z. B., Ed.; Springer-Verlag: Berlin, 1990; pp 339−386.
(19) Nixon, K L.; Wang, F.; Campbell, L.; Maddern, T.; Winkler, D.; Gleiter, R.; Loeb, P.; Weigold, E.; Brunger, M. J. *J. Phys. B* **2003**, *36*, 3155.
(20) Khajuria, Y.; Takahashi, M.; Udagawa, Y. *J. Electron Spectrosc. Relat. Phenom.* **2003**, *133*, 113.
(21) Chen, X. J.; Zhou, L. X.; Zhang, X. H.; Yin, X. F.; Xu, C. K.; Shan, X.; Wei, Z.; Xu, K. Z. *J. Chem. Phys.*. **2004**, *120*, 7933.
(22) Takahashi, M.; Ogino, R.; Udagawa, Y. *Chem. Phys. Lett.* **1998**, *288*, 714.
(23) Shan, X.; Chen, X. J.; Xu, C. K.; Zhou, L. X.; Xu, K. Z. *Chem. Phys. Lett.* **2006**, *422*, 246.
(24) von Niessen, W.; Brunger, M. J.; Weigold, E. *J. Phys. B* **1994**, *27*, 4309.
(25) Shan, X.; Chen, X. J.; Zhou, L. X.; Li, Z. J.; Liu, T.; Xue, X. X.; Xu, K. Z. *J. Chem. Phys.* **2006**, *125*, 154307.
(26) (a) Bawagan, A. O.; Muller-Fiedler, R.; Brion, C. E.; Davidson, E. R.; Boyle, C. *Chem. Phys.* **1980**, *120*, 335. (b) Rolke, A, J.; Zheng, Y.; Brion, Z.; Shi, Z.; Wolfe, S.; Davidson, E. R. *Chem. Phys.* **1999**, *244*, 1.
(27) Yang, B. X.; Chen, X. J.; Pang, W. N.; Chen, M. H.; Zhang, F.; Tian, B. L.; Xu, K. Z. *Acta Phys. Sin.* **1997**, *5*, 862.
(28) Weigold, E.; McCarthy, I. E. *Electron Momentum Spectroscopy*; Kluwer-Academic: New York, 1999.
(29) Minchinton, A.; Cook, J. P. D.; Weigold, E. *Chem. Phys.* **1987**, *113*, 251.
(30) Leung, K. T.; Brion, C. E. *Chem. Phys.*. **1985**, *95*, 241.
(31) Hamnett, S. T. A.; Brion, C. E. *Chem. Phys. Lett.*. **1976**, *41*, 428.
(32) Dey, S.; Dixon, A. J.; McCarthy, I. E.; Weigold, E. *J. Electron Spectrosc. Relat. Phenom.* **1976**, *9*, 397.
(33) Takahashi, M.; Ogino, R.; Udagawa, Y. *Chem. Phys. Lett.* **1998**, *288*, 821.
(34) Duffy, P.; Chong, D. P.; Casida, M. E.; Salahub, D. R. *Phys. Rev. A* **1994**, *50*, 4707, and references therein.
(35) Casida, M. E. *Phys. Rev. A* **2005**, *51*, 1995.
(36) Duffy, P. *Can. J. Phys.* **1996**, *74*, 763.
(37) Frisch, M. J.; Trucks, G. W.; Schlegel, H. B.; Scuseria, G. E.; Robb, M. A.; Cheeseman, J. R.; Zakrzewski, V. G.; Montgomery, J. A., Jr.; Stratmann, R. E.; Burant, J. C.; Dapprich, S.; Millam, J. M.; Daniels, A. D.; Kudin, K. N.; Strain, M. C.; Farkas, O.; Tomasi, J.; Barone, V.; Cossi, M.; Cammi, R.; Mennucci, B.; Pomelli, C.; Adamo, C.; Clifford, S.; Ochterski, J.; Petersson, G. A.; Ayala, P. Y.; Cui, Q.; Morokuma, K.; Malick, D. K.; Rabuck, A. D.; Raghavachari, K.; Foresman, J. B.; Cioslowski, J.; Ortiz, J. V.; Baboul, A. G.; Stefanov, B. B.; Liu, G.; Liashenko, A.; Piskorz, P.; Komaromi, I.; Gomperts, R.; Martin, R. L.; Fox, D. J.; Keith, T.; Al-Laham, M. A.; Peng, C. Y.; Nanayakkara, A.; Gonzalez, C.; Challacombe, M.; Gill, P. M. W.; Johnson, B.; Chen, W.; Wong, M. W.; Andres, J. L.; Gonzalez, C.; Head-Gordon, M.; Replogle, E. S.; Pople, J. A. *GAUSSIAN 98*; Gaussian, Inc.: Pittsburgh, PA, 1998.
(38) Becke, A. D. *J. Chem. Phys.* **1993**, *98*, 5648.
(39) Lee, C.; Yang, W.; Parr, R. G. *Phys. Rev. B* **1988**, *37*, 785.
(40) (a) Fleming, S. A.; Jensen, A. W. *J. Org. Chem.* **1996**, *61*, 7040. (b) Buell, S. L.; Demas, J. N. *Rev. Sci. Instrum.* **1982**, *53*, 1298.
(41) Novak, I.; Li, Org, D. B. *J. Chem* **2002**, *67*, 3510.
(42) Duffy, P.; Casida, M. E.; Brion, C. E.; Chong, D. P. *Chem. Phys.* **1992**, *159*, 347.
(43) Zhang, X. H.; Chen, X. J.; Xu, C. K.; Jia, C. C.; Yin, X. F.; Shan, X.; Wei, Z.; Xu, K. Z. *Chem. Phys.* **2004**, *229*, 14.